Journal of Power Sources 241 (2013) 33–45

Contents lists available at SciVerse ScienceDirect

Journal of Power Sources

journal homepage: www.elsevier.com/locate/jpowsour

Modeling the cathode pressure dynamics in the Buckeye Bullet II 540 kW hydrogen PEM fuel cell system

Edward T. Hillstrom [a], Marcello Canova [b,*], Yann Guezennec [b], Giorgio Rizzoni [b]

[a] Automotive Fuel Cell Cooperation, 9000 Glenlyon Parkway, Burnaby, BC V5J 5J8, Canada
[b] Center for Automotive Research, The Ohio State University, 930 Kinnear Road, Columbus, OH 43212, United States

HIGHLIGHTS

- High performance PEM fuel cell systems.
- Control-oriented model of PEMFC cathode pressure dynamics.
- Model of water transport in PEMFC cathode.
- Experimental validation on full-scale system.

ARTICLE INFO

Article history:
Received 3 October 2012
Received in revised form
12 March 2013
Accepted 18 March 2013
Available online 8 April 2013

Keywords:
Fuel cell systems
Modeling
Simulation
Control
Cathode pressure
Water management

ABSTRACT

The Buckeye Bullet 2 (BB2) is the world's fastest hydrogen fuel cell vehicle, with an international speed record of 302.9 mph. In order to achieve the power levels necessary for reaching the top speed, a unique gas supply system was designed to feed the PEM fuel cell modules. Stored Heliox with 40% oxygen content was used as the oxidizer and supplied to the cathode at high pressure. The high oxygen concentration at the cathode leads to a high rate of water formation in the GDL, with considerable influence on the pressure dynamics. For this reason, a precise monitoring of the pressure and water formation is required so that the cathode can operate at the maximum allowable pressure.

This paper presents a novel control-oriented modeling approach to predict the cathode pressure dynamics of the BB2 PEM fuel cell system, developed for system optimization, monitoring and control. A distributed-parameter model was designed to characterize the liquid water formation and transport in the cathode channels, starting from the conservation laws for viscous fluid flow.

The model was validated against a set of laboratory tests and actual race data. In this context, the proposed model is compared to a well known control-oriented PEM fuel cell model, to illustrate how the ability to predict the water transport at high reaction rates allows for an improved prediction of the pressure dynamics.

1. Introduction

On September 25th, 2009, the Buckeye Bullet 2 (BB2) became the first hydrogen fuel-cell vehicle to set an international speed record of 302.9 mph in the flying mile. The speed record was achieved at the end of a program that included over 2 years of initial conceptual design, followed by 3 years of testing, racing, and development.

Considerable research and development were devoted to the design, integration and power management of the propulsion system. To achieve the speed record, a power level of 540 kW was achieved by re-engineering the gas supply system of a Ballard PEM Fuel Cell Module (FCM) originally designed for 250 kW output.

Increasing the stack pressure and oxygen concentration in the feedgas are the most immediate ways to achieve high power output, however posing significant challenges to the fuel cell power management system. For instance attention must be paid to not exceed the pressure limits of the stack components, as the failure of a seal could lead to the leakage of fuel and oxidant. Furthermore, water formation and accumulation in the gas diffusion layer (GDL) has important effects on the pressure drop, creating obstruction to

* Corresponding author.
E-mail addresses: edward.hillstrom@afcc-auto.com (E.T. Hillstrom), canova.1@osu.edu (M. Canova), guezennec.1@osu.edu (Y. Guezennec), rizzoni.1@osu.edu (G. Rizzoni).

0378-7753/$ – see front matter © 2013 Elsevier B.V. All rights reserved.
http://dx.doi.org/10.1016/j.jpowsour.2013.03.103

the flow of reactants and, in some cases, leading to the flooding of a channel with consequent loss of power. This is particularly critical for the BB2 fuel cell system, where the pressurized oxygen-enriched reactant supplied to the cathode generates a significant amount of liquid water that must be expelled by controlling the pressure drop across the stack.

The case of the BB2 provides the opportunity to develop a control-oriented model predicting the water formation and transport through the stack channels at high current rates, and its impact on the cathode pressure dynamics. A robust and accurate cathode pressure dynamic model would be a powerful tool to facilitate the power management system design.

In this sense, many approaches for modeling the cathode pressure in PEM fuel cells have been proposed. The simplest models developed consist of a quasi-static approximation of the fuel cell polarization curve, based on a set of algebraic expressions for the thermodynamic equilibrium potential, along with activation, ohmic, and mass transport losses [1–4]. This model was further extended to account for transient behavior [5], to incorporate voltage degradation due to aging [6], and to include the anode activation losses [7], which are typically ignored in fuel cell modeling.

More accurate models are based on applying the conservation laws to a reacting two-phase flow in the stack channels. The problem is intrinsically multi-dimensional, multi-scale and time varying, therefore requiring solution of coupled partial differential and algebraic equations [8–29].

In this scenario, the prediction of water formation and transport in the Gas Diffusion Layer (GDL) is a considerable research challenge, and several contributions have been made in the development of first-principle models, for instance [30–32]. Recently, a multi-dimensional modeling approach was proposed in Ref. [33] to explore the operations of PEM fuel cells at high current density conditions. Here, predicting the water balance across the membrane and the transport along the channels is critical to elucidate performance limitations at ultra-high current density operations.

While such models provide very accurate results when compared with experimental data, in many practical applications simple one-dimensional (1D) modeling approaches are adopted in light of their relative simplicity and reduced computation time. Based on the 1D modeling approach, the fuel cell cathode is simplified to a single flow channel, and the fundamental equations are discretized along the length of the channel, using a variety of assumptions to model the exchange of current and mass through the membrane.

Common assumptions include isothermal conditions, and a constant pressure along the flow channel. For instance, isothermal 1D models were proposed in Refs. [34,35], focusing on predicting the water transport along the length of the flow channel for determining optimal membrane humidification levels. A different approach was proposed in Refs. [36], consisting of solving the 1D current and mass transfer in the membrane off-line and generating a look-up table that can be used to solve a 1D model of the channel [37].

The use of the 1D approach often involves solving coupled linear and non-linear partial differential equations that may contain discontinuous terms, which typically require complex numerical solution techniques that are computationally expensive. Despite the simplifications that can be introduced, 1D methods do not lead to control-oriented model that are simple enough to be used for control design.

Compared to first-principle models, relatively little is available in the open literature on fuel cell models oriented to system-level optimization and control design. Possibly the most commonly referenced work in this area was developed in Refs. [38–41], and relies on a lumped-parameter approximation of the fuel cell stack and air supply system into a set of interconnected control volumes. Under isothermal conditions, the mass balance equation is solved accounting for the chemical reactions that consume reactants and produce water. Linear flow resistance terms are introduced to connect the control volumes (inlet, cathode and exhaust), thereby leading to determining the mass flow rates and cathode pressure. Another lumped parameter model was proposed in Refs. [42], and considered the temperature and thermal effects for three separate control volumes, namely the anode, cathode, and the membrane-electrode assembly (MEA).

While lumped-parameter models are largely in use to facilitate control design, they rely on simplifying assumptions that make them unsuited for capturing the behavior of high performance fuel cells, such as the BB2 system. For instance, the presence of liquid water in the cathode does not affect the pressure drop through the cell, which is essentially assumed only a function of the gas phase [38]. In reality, water formation has significant effects on the pressure drop at high current density, creating obstruction to the flow of reactants and, in some cases, resulting in flooding of one or more cells.

To this extent, this paper presents a novel modeling approach to predict the cathode pressure dynamics at high current density conditions, designed for high performance PEM fuel cell system such as in the Buckeye Bullet 2. A significant improvement from well-established control-oriented cathode pressure models (such as the one proposed in Ref. [38]), the water formation and transport in the cathode is here explicitly characterized through a physics-based distributed-parameter model, leading to an improved accuracy in predicting the pressure dynamics during load transients. At the same time, the resulting model is computationally very efficient and suitable for model-based control design.

In this paper, the developed model is compared to the modeling approach proposed [38–41], specifically adapted to the fuel cell system of the BB2. Both models were calibrated and validated using experimental data collected on laboratory tests and actual race data. A comparison of the cathode pressure response predicted by the two models for a transient load current input allows one to understand how a correct prediction of the water formation and transport dynamics at high current density conditions leads to an improved prediction of the cathode pressure.

The paper is organized as follows. First, an overview of the Buckeye Bullet 2 fuel cell propulsion system is presented. Then, two modeling approaches are discussed, namely the conventional control-oriented fuel cell model and then the novel, distributed-parameter cathode pressure model. A description of the experimental setup built for collecting data is illustrated next, outlining the available measurements, the methodology for parameter calibration, and the calibration results. Finally, validation results are presented to illustrate how the two models compare in predicting the cathode pressure dynamics at high current density operations.

2. System description

The Buckeye Bullet 2 land speed record vehicle architecture is shown in Fig. 1. Two high pressure hydrogen fuel tanks are located at the rear, with the driver in front of the fuel cells, separated by a firewall from the hydrogen gas systems. The fuel cells power the front AC induction motor connected to a six-speed transmission. The low profile motor allows for the driver head to be lowered, hence reducing the frontal area and the aerodynamic drag. A four-wheel independent suspension system was designed to control the stability over a variety of track conditions. The primary method to stop the vehicle is with the use of 2 high-speed parachutes. The

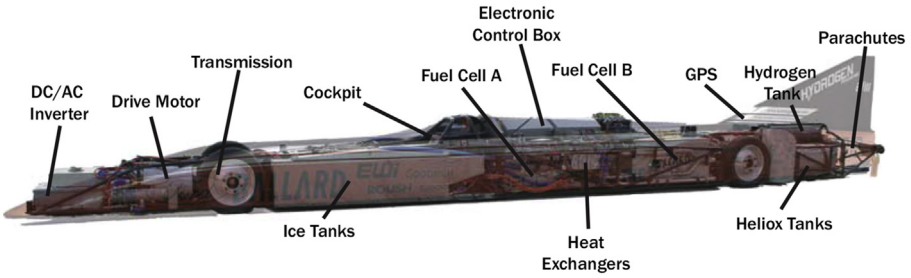

Fig. 1. Architecture of the Buckeye Bullet 2 land speed vehicle.

vehicle also has Lear-jet aircraft brakes at all wheels that could stop the vehicle in an emergency situation or parachute failure.

The gas supply system is shown in Fig. 2. The hydrogen is supplied to the anode at high pressure, with a recirculation system routing the unreacted gas to the stack inlet via a multistage ejector pump. During normal operations, water and other inert gases can accumulate in the fuel loop, requiring periodic purging. Hydrogen fuel pressure and flow are controlled passively using a pressure regulator externally piloted by the air delivery system to balance the air and hydrogen pressures across the fuel cell membrane.

Typical PEM fuel cell vehicles are designed to use ambient air as the oxidizer. A compressor driven by an electric motor supplies air at the desired inlet pressure to the stack, leading to a parasitic loss of up to 20% of the power produced [43]. For a land speed vehicle, such parasitic load would severely affect the acceleration and top speed, particularly considering the short duration of a speed run (about 90 s). For this reason, a stored oxidizer supply system was designed, allowing for higher gas pressure and oxygen concentration. Heliox (60% helium and 40% oxygen), stored at 220 bar, was chosen as a trade-off between maximum system performance and safety.

The fuel cell system, shown in Fig. 3, consists of two Ballard P5 Fuel Cell Modules (FCMs), each formed by 960 cells in series, connected in parallel. The cathode supply system for the two FCMs is operated in parallel with a shared exhaust and pressure regulation system. From the storage tanks, the gas is regulated to 10 bar just upstream of the two mass flow controllers. The cathode gases flow into each FCM, where they pass though a humidifier before entering the stacks. The enriched oxygen concentration reduces the voltage losses at high current draws. Downstream of the stacks, the gases are combined in a shared exhaust volume.

The gas flow system is controlled to supply oxygen to the stacks and assist in the removal of the water. The flow rate of the Heliox is regulated by two mass flow controllers (MFC), while the stack pressure is set through three Pressure Regulation Valves (PRV). Due

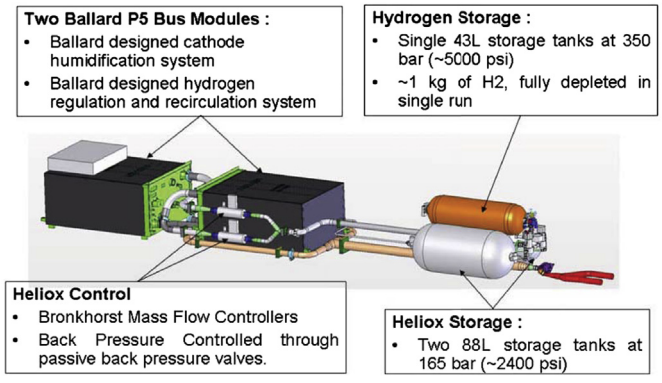

Fig. 2. Overview of the BB2 hydrogen and Heliox supply system.

to the high current drawn from the stacks (about 400 A per module) and the high inlet oxygen concentration, water removal is a significant challenge.

An additional control challenge lies in the presence of a manual transmission, which causes a very dynamic change in the current draw at each shift. While the fuel cells are operated at maximum power during the acceleration phase, a short drop to zero current occurs at each gear shift. The sudden change in current causes rapid fluctuations in the rate of reaction and, consequently, in the rate of water formation. This may lead to cathode pressure spikes, requiring control of the back pressure valves to compensate the rapid changes in the gas concentration.

3. Model development

The starting point for modeling the cathode pressure dynamics of the BB2 fuel cell is the control-oriented model developed in Refs. [38], where the system is divided into a cathode volume (where the reactions occur) and an exhaust volume. The aforementioned model was adapted to the BB2 system by separately modeling the two fuel cell modules, each subject to different oxidizer flow and current inputs.

A new distributed-parameter model was then developed to specifically include the ability to predict the dynamics of the water formation and transport in the cathode channels, as well as the effect of water liquid and vapor on the pressure drops across the cathode.

3.1. Lumped-parameter (simplified) model equations

An initial attempt to predict the cathode pressure dynamics was made by applying the modeling approach described in Ref. [38].

Fig. 4(a) describes the block diagram of the model of the BB2 fuel cell system, consisting of two modules feeding a common exhaust manifold. Each module is represented by a lumped-parameter model according to the block diagram shown in Fig. 4(b). Specific submodels determine the composition of the inlet and outlet flows (helium, oxygen, water) based on the conservation laws for reacting systems. The stack pressure is then calculated from the mass conservation and the ideal gas law.

The *Inlet Flow* and *Humidifier* block computes the composition of the reactants to the cathode, based on the measured flow rate of Heliox and the desired relative humidity. The mass flow rate of water injected at the cathode inlet, $W_{v,ca,in}$, is defined as follows:

$$W_{v,ca,in} = \frac{M_v}{M_{\text{Heliox}}} \frac{\phi_{\text{des}} \cdot P_{\text{sat}}(T)}{P_{ca}} W_{\text{MFC}} \quad (1)$$

where M denotes the molecular weight, ϕ is the desired relative humidity, which for the BB2 system is assumed to be 100% (saturated conditions). The water injected by the humidifier is assumed

to be in saturated vapor form, whose saturation pressure P_{sat} (kPa) is a function of the operating temperature (K) [44]:

$$\log_{10}(P_{sat}) = -1.69\cdot10^{-10}T^4 + 3.85\cdot10^{-7}T^3 + -3.39\cdot10^{-4}T^2 + 0.143T - 20.92 \quad (2)$$

The *Electrochemistry* block calculates the oxygen consumption and water formation based on the current drawn:

$$W_{o,\text{reacted}} = M_o\cdot\frac{nI_{st}}{4F}$$
$$W_{v,\text{gen}} = M_v\cdot\frac{nI_{st}}{2F} \quad (3)$$

where I_{st} is the input current to the stack and F the Faraday constant.

The *Cathode Mass Balance* block applies the conservation of mass to track the composition of the mixture, specifically oxygen (o), helium (h) and water (denoted with v for the vapor phase and L for the liquid phase):

$$\frac{dm_{o,ca}}{dt} = W_{o,ca,in} - W_{o,ca,\text{out}} - W_{o,\text{reacted}}$$
$$\frac{dm_{h,ca}}{dt} = W_{h,in} - W_{h,\text{out}}$$
$$\frac{dm_{v,ca}}{dt} = W_{v,ca,in} - W_{v,ca,\text{out}} + W_{v,\text{gen}} - W_{v,\text{cond}} \quad (4)$$
$$\frac{dm_{L,ca}}{dt} = W_{v,\text{cond}} - W_{L,ca,\text{out}}$$

Since the gas mixture at the cathode inlet is in saturation condition, the formation of liquid water is tracked by calculating the maximum mass of water vapor that can be held in the cathode:

$$m_{v,\max} = \frac{P_{\text{sat}}(T)V_{ca}}{R_vT} \quad (5)$$

where V_{ca} is the cathode volume, R_v is the specific gas constant for water vapor and the saturation pressure is calculated according to Equation (2). To this end, a simplifying assumption is introduced, in that the water in the cathode forms first in vapor form, and then condenses based on the thermodynamic conditions of the mixture. The flow rate of condensate $W_{v,\text{cond}}$, is therefore defined as follows:

$$W_{v,\text{cond}} = \begin{cases} 0 & \text{if } m_{v,ca} < m_{v,\max} \\ W_{v,\text{gen}} & \text{if } m_{v,ca} \geq m_{v,\max} \end{cases} \quad (6)$$

A critical assumption made in Ref. [38] is that the liquid water generated does not affect the cathode pressure. Therefore, the cathode pressure P_{ca} is calculated in the *Thermodynamic Calculations* block by using the Dalton's law:

$$P_{ca} = \sum_i P_i, \quad P_i = \frac{m_{i,ca}R_iT}{V_{ca}} \quad (7)$$

where $i = (o,h,v)$. Note that the cathode volume is here assumed constant, which is a consequence of neglecting the effects on the pressure of the liquid water formed in the cathode.

The *Stack Resistance* block calculates the mass flow rate exiting the cathode, based on a linearized resistance that lumps the distributed and concentrated losses through the stack [41]:

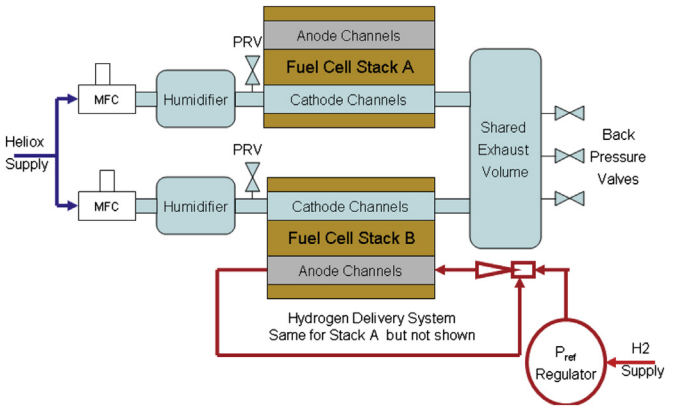

Fig. 3. Schematic of the BB2 fuel cell system.

$$W_{ca,\text{out}} = K_{\text{stack}}(P_{ca} - P_{em}) \quad (8)$$

where P_{em} is the exhaust manifold pressure (common to the two modules), and the parameter K_{stack} is calibrated based on experimental data.

The assumption of a linear flow resistance made in Ref. [41] could be in part justified by the fact that the BB2 fuel cell mostly operates a full load, hence nearly in steady-state conditions. Further, the stack channels operate predominantly under laminar flow conditions, under a relatively small pressure ratio.

The *Outlet Flow Properties* block calculates the mass flow rate of each mixture component out of the cathode channels, based on the mass fraction:

$$X_i = \frac{m_{i,ca}}{\sum_i m_{i,ca}}, \quad W_{i,ca,\text{out}} = X_i\cdot W_{ca,\text{out}} \quad (9)$$

where i = o,h,v.

The same modeling approach is applied to the exhaust manifold, wherein the composition of the mixture is given by the mass conservation equation and the mass flow rates coming from the two fuel cell modules. In order to meet the flow rate requirements, three Fischer 289H passive Back Pressure Valves (BPV) are used in parallel to regulate the stack pressure. The valve is internally piloted, and adjustable to various pressure settings through a spring-diaphragm system. A static model of the BPV was developed starting from the OEM data sheet shown in Fig. 5. The flow map provides lines describing the relationship between the volumetric flow rate and the inlet pressure to the valve, for a variety of preset pressure settings. A correction factor K_{BPV}, which multiplies the flow rate from the characteristic map, is then introduced to account for the variation of the Specific Gravity (SG) of the gas mixture, which is defined as the ratio between the density of the gas in the exhaust manifold and the density of air. The correction factor is calibrated on experimental data. Using the notation in Fig. 4(c), the final model for the three BPV in parallel can therefore be expressed in implicit form:

$$W_{em,\text{out}}(t) = 3K_{\text{BPV}}\cdot\frac{P_{em}}{RT}\cdot Q_{\text{BPV}}(P_{em}(t), P_{\text{preset}}) \quad (10)$$

where Q_{BPV} is the volumetric flow rate through one valve, K_{BPV} and P_{preset} are calibration parameters.

3.2. Distributed-parameter model equations

As mentioned above, the simplified lumped-parameter fuel cell model ignores much of the complexity in the BB2 fuel cell system,

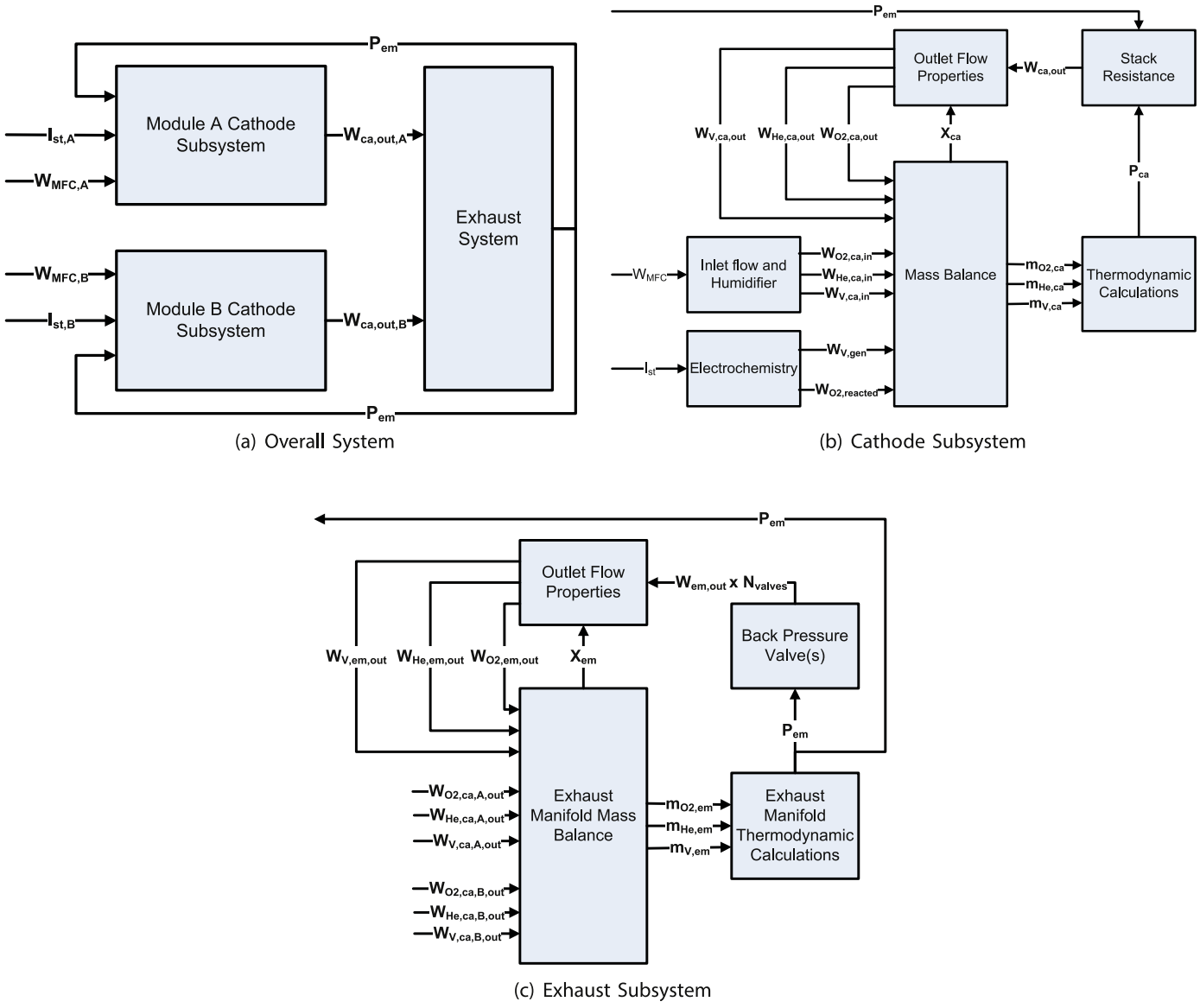

Fig. 4. Block diagrams showing the input/output structure of the BB2 fuel cell system model. (a) Overall system, (b) cathode subsystem, (c) exhaust subsystem.

particularly the effects of the complex geometry of the inlet and exhaust manifolds on the cathode pressure drop, as well as the effects of the liquid water formation and transport on the cathode pressure dynamics.

For the above reasons, a novel distributed-parameter model characterizing the flow of reactants and products at the cathode side was developed by inspecting the gas flow path through the cathode and deconstructing the system into a set of interconnected control volumes. Fig. 6 provides a schematic representation of the gas flow path through the complete stack.

The feedgas first enters an inlet manifold, where is directed to each of the 6 cell rows. The gas then travels down a runner within each cell row, where it enters the channels. Significant restrictions are encountered as the gas is separated into each channel.

The gas faces another significant restriction at the exit of the channel, where it recombines into the runner and, ultimately, in the manifold to a single outlet. In this case, the pressure drop through the exit restriction is largely dependent on the mixture composition, and particularly on the rate at which liquid water exits the cathode channels.

Based on the system topology described above, Fig. 7 shows the block diagram of the proposed cathode pressure model. Compared to the simplified model shown in Fig. 4, the inlet manifold, inlet flow resistance and exit flow resistance are now formally accounted for. In addition, a more complex model was developed to characterize the formation and transport of liquid water in the cathode channels, and its effects on the pressure drop.

Modeling the water formation and transport is quite complex. In general, a two-phase flows originates from water droplets forming on the hydrophobic Gas Diffusion Layer (GDL), which then entrain and disperse into the gas flow [30,32]. On the other hand, the developed model simplifies the complex physics of the problem by assuming that liquid water forms as a film along the channel walls, and is subsequently transported by the gas phase through drag forces. The above assumption can in part be justified by the large quantity of water that is produced in the BB2 fuel cells, due to the oxygen-enriched feedgas and the very high current density [33].

The equations describing the motion of the gas and liquid phase are based on the theory for incompressible viscous fluid flow in a 1D channel [45]. Limiting the analysis to a small element of the

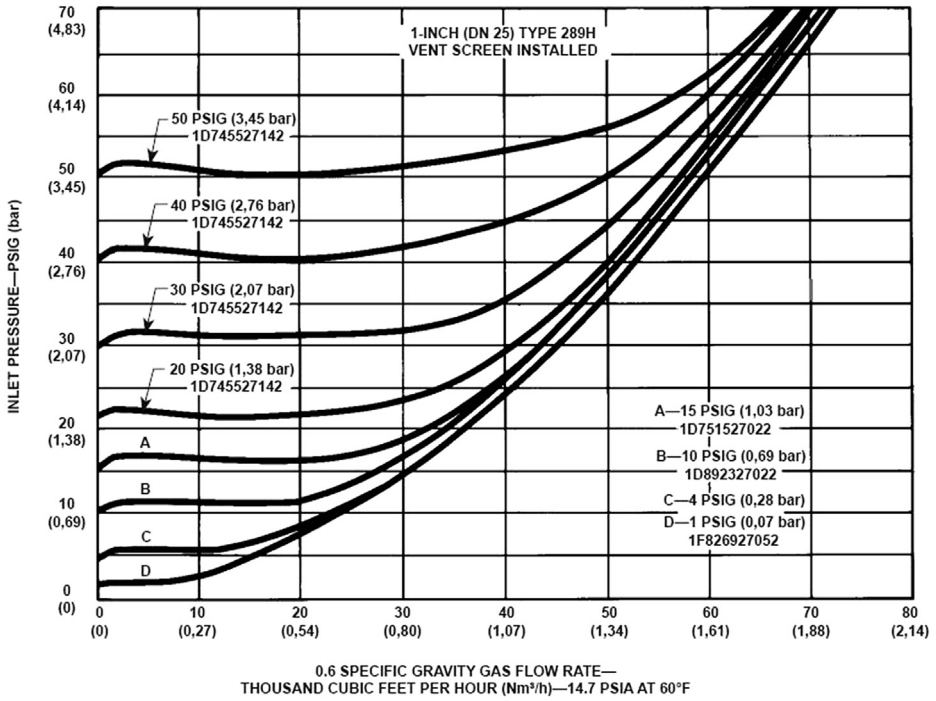

Fig. 5. Back pressure valve performance map (0.6 SG dry gas).

cathode channel, it is possible to assume that the gas and liquid flows are separated by an interface parallel to the direction of the flow, as shown in Fig. 8.

Using the notation in figure, the velocity profiles for the liquid and gas phase are obtained by solving the Navier–Stokes equations for steady-state, fully developed laminar flow in a cell of length dx [45]:

$$\begin{aligned} u_L(x,y) &= \frac{1}{2\mu_L}\left(\frac{\partial P}{\partial x}\right) y^2 + \frac{c_{1L}}{\mu_L} y + c_{2L} \\ U_g(x,Y) &= \frac{1}{2\mu_g}\left(\frac{\partial P}{\partial x}\right) Y^2 + \frac{c_{1g}}{\mu_g} Y + c_{2g} \end{aligned} \tag{11}$$

where L refers to the liquid domain and g to the gas domain within the cell, and P is the pressure varying along the flow direction x. The integration constants $c_{1L},\ldots,c_{2g}$ are found by imposing no-slip boundary conditions at the walls and equal shear stress at the interface. A slip condition is however considered at the interface, and the slip factor is assumed a calibration parameter. The complete set of boundary conditions is expressed as follows:

$$\begin{cases} u_L(x,0) = 0 \\ U_g(x,0) = 0 \\ u_L(x,h) = \alpha \cdot U_g(x,H) \\ \mu_L \cdot \dfrac{\mathrm{d}u_L}{\mathrm{d}y}\Big|_{x,y=h} = \mu_g \cdot \dfrac{\mathrm{d}U_g}{\mathrm{d}Y}\Big|_{x,Y=h} \end{cases} \tag{12}$$

Substituting Equation (12) into (11) and manipulating the resulting expression, the flow velocity of the gas and liquid phase are given by:

$$\begin{aligned} u_L(x,y) &= \left(\frac{\partial P}{\partial x}\right)\left[\frac{1}{2\mu_L} y^2 + \frac{CC_L}{\mu_L} y\right] \\ U_g(x,Y) &= \left(\frac{\partial P}{\partial x}\right)\left[\frac{1}{2\mu_g} Y^2 + \frac{CC_g}{\mu_g} Y\right] \end{aligned} \tag{13}$$

where the parameters CC_L and CC_g are equal to:

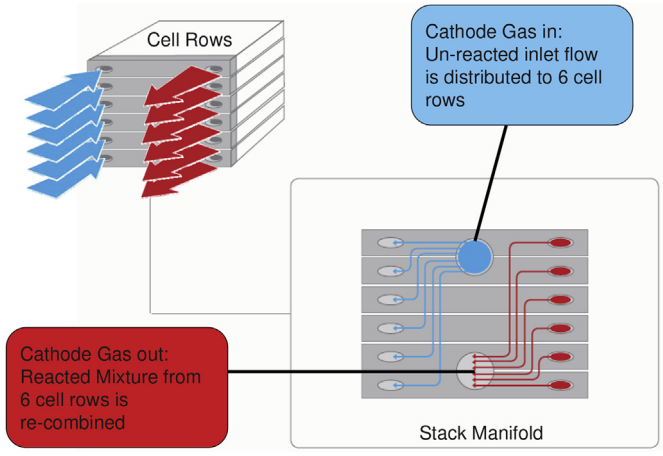

(a) Schematic of Stack Manifold

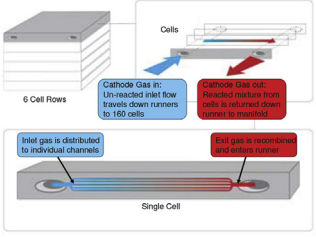

(b) Schematic of an Individual Cell Row

Fig. 6. Schematic illustrating the feedgas flow path through the BB2 fuel cell stack. (a) Schematic of stack manifold, (b) schematic of an individual cell row.

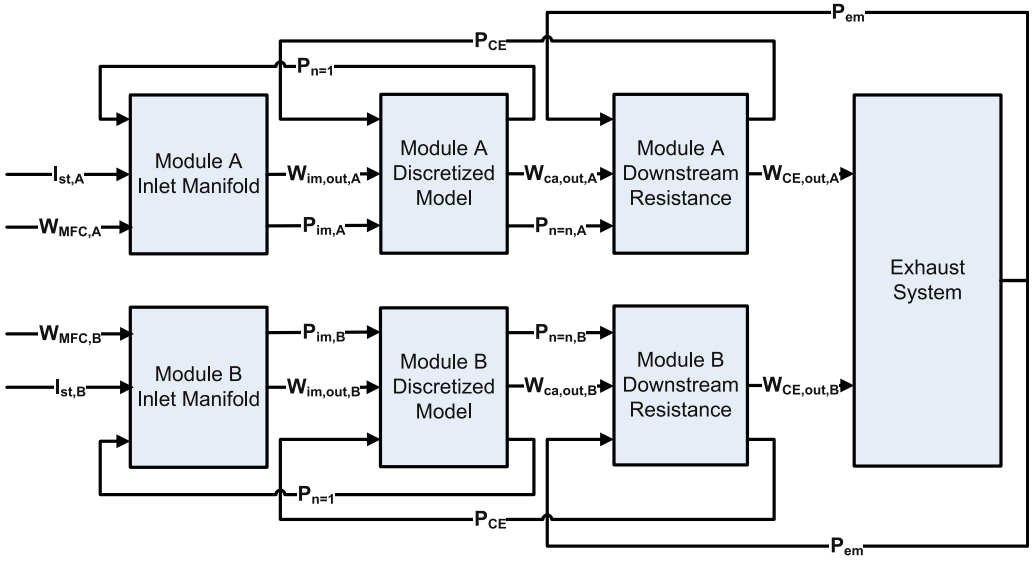

Fig. 7. Block diagram of the distributed-parameter cathode model.

$$CC_L = \frac{\frac{\alpha H h}{\mu_g} - \frac{h^2}{2\mu_L} - \frac{\alpha H^2}{2\mu_g}}{\frac{h}{\mu_L} - \frac{\alpha H}{\mu_g}}$$
$$CC_g = \frac{-\frac{Hh}{\mu_L} + \frac{h^2}{2\mu_L} + \frac{\alpha H^2}{2\mu_g}}{\frac{h}{\mu_L} - \frac{\alpha H}{\mu_g}} \quad (14)$$

The velocity profiles are then integrated to determine the mass flow rate for the gas and the liquid phase. To this extent, a discretization is operated on Equation (11) to approximate the pressure gradient. Considering a square channel of width w, the mass flow rates in the generic element $n = 1,\ldots,z$ of the channel are given by:

$$W_{L,n} = \rho_L w\left(\frac{P_n - P_{n+1}}{\Delta x}\right)\left[\frac{1}{6\mu_L}h_i^3 + \frac{CC_{L,n}}{2\mu_L}h_n^2\right]$$
$$W_{g,n} = \rho_g w\left(\frac{P_n - P_{n+1}}{\Delta x}\right)\left[\frac{1}{6\mu_g}H_n^3 + \frac{CC_{g,n}}{2\mu_g}H_n^2\right] \quad (15)$$

where $\Delta x = L_{\text{channel}}/z$.

Note that the height h and H of the liquid and gas phase are linearly dependent, since $(h + H) = w$. Therefore, the model here developed results into a set of purely algebraic equations:

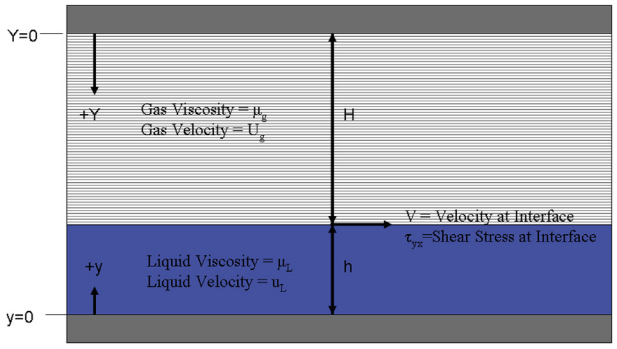

Fig. 8. Representation of two-phase laminar flow in a 1D channel.

$$W_{L,n},\ W_{g,n} = f_i(P_n, P_{n+1}, h_n) \quad (16)$$

which is analogous to the quasi-static nonlinear expressions for flow restrictions.

In order to solve the above model, it is necessary to include a set of differential equations defining the state variables for the system, namely the time-varying pressure P_n and liquid height h_n in each element in the channel.

This can be easily done by modifying Equation (4), which expresses the conservation of mass for a gas mixture in control volume with electrochemical reactions. Fig. 9 shows a simple schematic of the discretization operated on the cathode channel, while Fig. 10 illustrates the block diagram representation for the model.

Assuming isothermal conditions, the mass balance equations for the three gaseous species and liquid water are:

$$\frac{dm_{o,n}}{dt} = W_{o,\text{out},n-1} - W_{o,\text{out},n} - W_{o,\text{reacted},n}$$
$$\frac{dm_{h,n}}{dt} = W_{h,\text{out},n-1} - W_{h,\text{out},n}$$
$$\frac{dm_{v,n}}{dt} = W_{v,\text{out},n-1} - W_{v,\text{out},n} + W_{v,\text{gen},n} - W_{v,\text{cond},n} \quad (17)$$
$$\frac{dm_{L,n}}{dt} = W_{L,\text{out},n-1} - W_{L,\text{out},n} + W_{v,\text{cond},n}$$

where, assuming a uniform current distribution through the length of the channel, the terms depending on the electrochemical reactions are still defined based on Equation (3), however divided by the number of elements z.

Given the mass flow of liquid in the channel element, the channel height and the volume occupied by the gas are given by:

$$h_n = \frac{m_{L,n}}{w\rho_L\Delta x}$$
$$V_{g,n} = (w - h_n)w\Delta x \quad (18)$$

where ρ_L is the density of the liquid water.

Finally, the pressure within the n-th element of the channel is computed from the partial pressures of the gas components and the actual volume occupied by the gas:

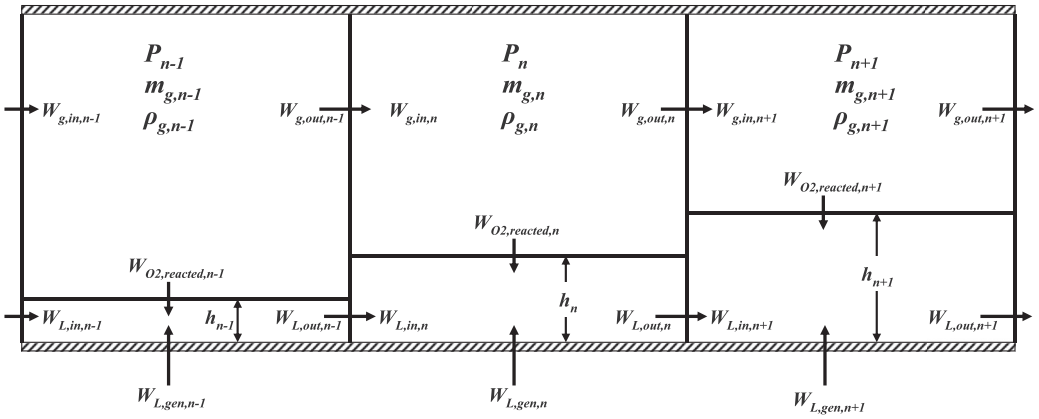

Fig. 9. Schematic of discretized cathode channel.

$$P_n = \sum_i P_{i,n}$$
$$P_{i,n} = \frac{m_{i,n} R_i T}{V_{g,n}}, \quad i = (o, h, v) \tag{19}$$

Based on Fig. 7, two more equations are needed to connect the distributed-parameter cathode model to the inlet manifold and the exhaust system models. These equations are based on the pressure drop characteristics of the flow restrictions upstream and downstream the cathode.

At the cathode inlet, a concentrated loss is considered to predict the pressure drop through the inlet runners, as shown in Fig. 6. Since the fluid flow at the cathode inlet is a saturated mixture of Heliox and water vapor, a simple linear flow resistance is assumed for calculating the gas flow rate to the two fuel cell modules:

$$W_{im,out} = K_{US}(P_{im} - P_{n=1}) \tag{20}$$

where K_{US} is a calibration parameter and $P_{n=1}$ is the gas pressure within the first element of the channel. From the above equation, the mass flow rate of the individual components is computed based on the known mass fractions of helium, oxygen and water vapor in the inlet manifold. This allows one to apply the mass balances in Equation (17) and solve for the pressure $P_{n=1}$.

On the other hand, the resistance to the flow downstream the cathode is significantly affected by the presence of liquid water in the stream. In order to determine a physically accurate but manageable expression for the pressure drop, a simplified approach is taken, based on the semi-empirical correlations for two-phase flows [46]:

$$\Delta P = P_{n=z} - P_{em} = W_{CE,\text{out}}^2 K_{DS}\left[\frac{X}{\rho_g} - \frac{(1-X)}{\rho_L}\right] \tag{21}$$

where $W_{CE,\text{out}}$ is the mass flow rate of the stream (liquid, gas and water vapor) exiting the last cathode element, X is the mass fraction of water vapor contained in the stream, and ρ_g refers to density of the gas phase, Similar to the cathode inlet resistance, the parameter K_{DS} is determined through calibration. The above expression can be inverted to output the flow rate as function of the pressure difference between the last cathode element and the exhaust manifold. Once again, the above expression is applied to each of the two modules.

4. Description of the experimental setup

In order to validate the distributed-parameter cathode pressure model and provide a comparison against the simple control-

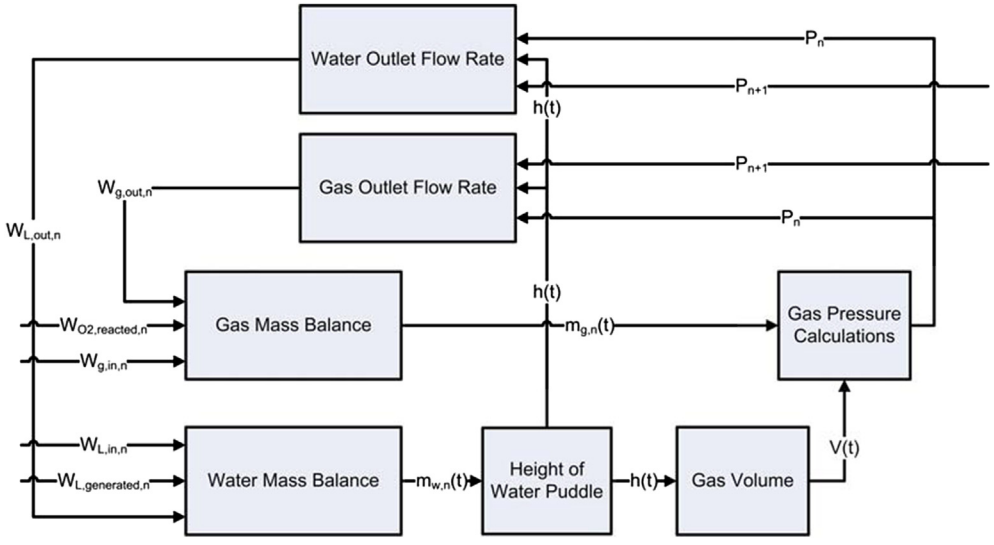

Fig. 10. Block diagram representation of one channel element.

Fig. 11. Overview of the resistive load bank for electrical testing.

oriented model, a laboratory setup was engineered to allow for testing the BB2 fuel cell system on operating conditions as close as possible to an actual race. In order to test the system at full power conditions without committing to a powertrain dynamometer or full vehicle testing, the power output of the fuel cells was diverted from the inverter/motor and dissipated on a programmable electrical load.

To this end, a load bank was designed by assembling 9 resistors in parallel, with switches that can be controlled to dynamically vary the electrical resistance of the circuit. A ducted ventilation system powered by a 15HP AC induction motor was built to provide sufficient cooling flow to the resistors. Fig. 11 illustrates the setup, while Table 1 lists the values of the individual resistances and the equivalent resistance and bank current when the resistors are progressively connected.

By controlling the switches, it was possible to reproduce the current profile that the fuel cells would be subject to during typical racing conditions. Since the resistors could only be switched in 9 discrete steps, current ramps could be only approximated as staircase profiles. To simulate the sudden current drop during a gear shift, all switches were cut simultaneously and then connected to full current in about 1 s. Fig. 12 compares the current profile for the two fuel cell modules during racing conditions with the optimized profile obtained on the load bank.

For the fuel cell system tests, the available measurements included mass flow rate at the cathode and anode side, relative humidity in the intake manifold, stack current and voltage, and temperature at several locations. Pressure sensors were installed upstream and downstream of the cathode. The Ballard fuel cell control system was also available to monitor the voltage of the individual channels and to override the production control system if needed.

A water collection system was designed to measure the water mass flow rate expelled. As shown in Fig. 13, the exhaust was routed to a large basin posed on a digital scale. A correction term was introduced to remove the effects of the aerodynamic forces acting on the scale due to the high exit velocity of the exhaust gases.

Table 1
Resistance levels and currents for the load bank.

Switch #	Ω_{switch}, ohms	Ω_{total}, ohms	I_{bank}, A
1	7.80	7.80	55
2	6.16	3.44	115
3	6.16	2.20	172
4	6.16	1.62	226
5	6.16	1.29	277
6	5.10	1.02	334
7	5.10	0.85	388
8	5.10	0.73	440
9	5.10	0.64	480

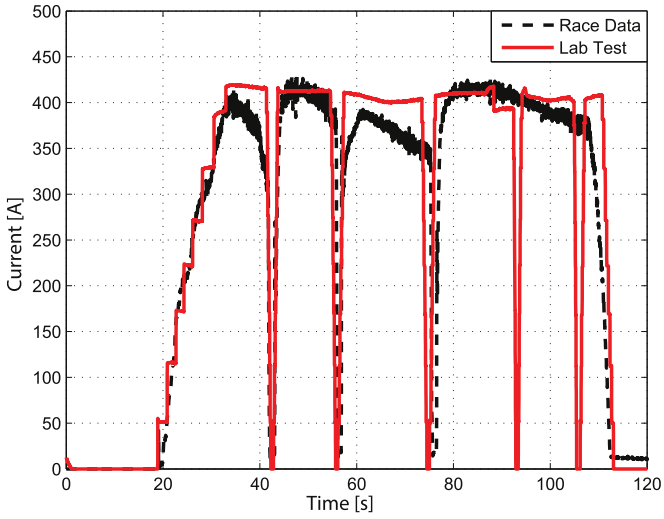

Fig. 12. Verification of current profile obtained with the load bank.

5. Results and analysis

For the calibration and validation of the two models, two different experimental tests were conducted. The stack current profile during each test is shown in Fig. 14. In the first test, a near-constant stack current was imposed and held as long as possible. The second test was conducted by starting with a nominally constant stack current profile, then controlling the resistive load bank to impose three consecutive rapid drops in stack current and power output. This profile introduces some of the fast transients that the fuel cell system experiences when a gear shift occurs during a race. Both tests were done at a nominally constant stack current and voltage, to represent the typical operating conditions during a race.

For both tests, the region of interest for the calibration and validation of the two models corresponds to the cell operating at nominally constant stack current, hence at near steady-state conditions. In Fig. 14, this region starts approximately at 10 s and ends at about 90 s.

Since the stack current as well as the flow rates of hydrogen and Heliox are constant during this phase, the parameters of the two models can be identified to constant values, hence simplifying the calibration process. Therefore, the results presented here may be extended to different operating conditions, by further calibrating the parameters as functions of the measured mass flow rates of reactants.

5.1. Calibration results

The calibration was conducted using the experimental data collected on the constant current profile shown in Fig. 14(a).

The parameters considered for the simplified, lumped-parameter model (indicated with LPM in the following discussion), are the flow resistance coefficient downstream the cathode, K_{DS}, the correction factor for the back pressure valve flow, K_{BPV} and the preset pressure P_{preset}.

For the distributed-parameter model (DPM), which includes the model of the water and gas transport in the channels, two additional parameters, namely a flow resistance coefficient upstream of the cathode (K_{US}), and the slip factor α at the liquid–gas interface, require calibration.

Prior to the calibration, a sensitivity study was conducted on the DPM to determine the influence of the discretization length of the cathode channel model on the outputs. In particular, seven

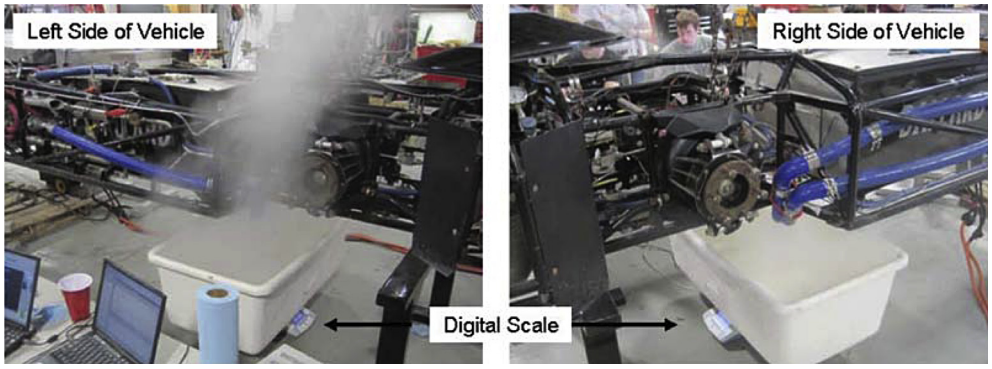

Fig. 13. Water measurement test setup.

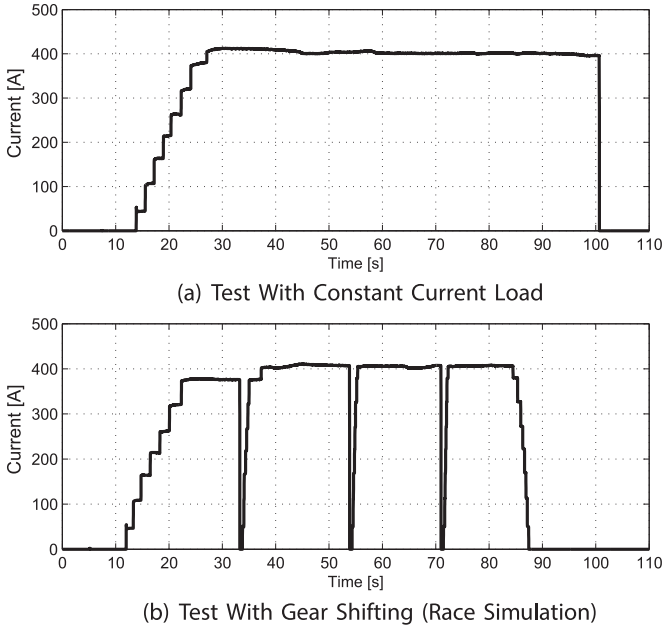

Fig. 14. Current profiles for model calibration and validation. (a) Test with constant current load, (b) test with gear shifting (race simulation).

elements were found as the condition for which the predicted mass flow rate of liquid water exiting the cathode becomes insensitive to the grid size.

The parameters were calibrated by setting a nonlinear optimization problem that minimizes the error function:

$$p^* = \arg\min \left[\int_{t_1}^{t_2} \frac{\|\Delta P_{\text{data}}(t) - \Delta P_{\text{model}}(t)\|}{t_2 - t_1} \right] \tag{22}$$

where p is the parameter set of each model and ΔP is the pressure drop through the cathode. Tables 2 and 3 summarize the values of the optimized parameters for the two models.

The two models were simulated by imposing the stack current, as well as the flow rate and initial composition of the Heliox fed to

Table 2
Calibration parameters for the LPM.

Parameter	Value	Units
P_{preset}	31	psi
K_{BPV}	0.25	–
K_{DS}	$1.8e^{-6}$	kg (Pa–s)$^{-1}$

Table 3
Calibration parameters for the DPM.

Parameter	Value	Units
P_{preset}	28.5	psi
K_{BPV}	0.25	–
K_{US}	$5.1e^{-6}$	kg (Pa–s)$^{-1}$
K_{DS}	2000	1 (m^2 kg)$^{-1}$
α	1	–

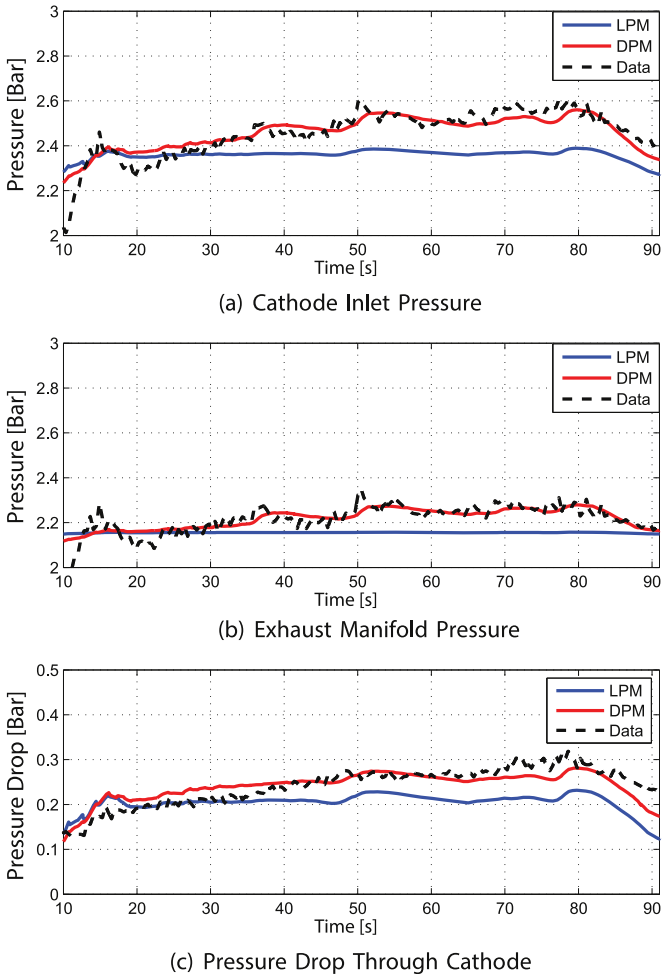

Fig. 15. Comparison of LPM and DPM predictions: calibration results. (a) Cathode inlet pressure, (b) exhaust manifold pressure, (c) pressure drop through cathode.

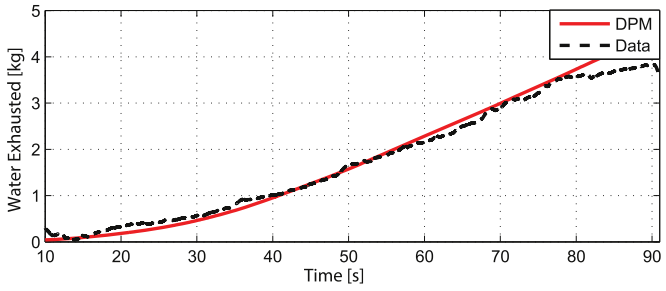

Fig. 16. Mass of liquid water produced during calibration test.

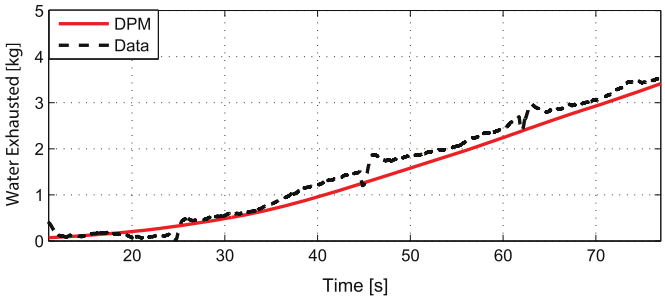

Fig. 18. Mass of liquid water produced during validation test.

Table 4
Comparison of LPM and DPM performance for calibration set (Fig. 14(a); test duration: 90 s).

	Error on inlet pressure (bar)	Error on exhaust pressure (bar)	Error on pressure drop (bar)	Number of states (−)	Comp. time (s)
LPM	0.119 (4.5%)	0.075 (3.2%)	0.045 (14.5%)	9	2.8
DPM	0.030 (1.2%)	0.022 (0.9%)	0.017 (5.4%)	30	15.1

the cathode. The predicted pressures at the cathode inlet and outlet, as well as the overall pressure drop are compared to the measured data.

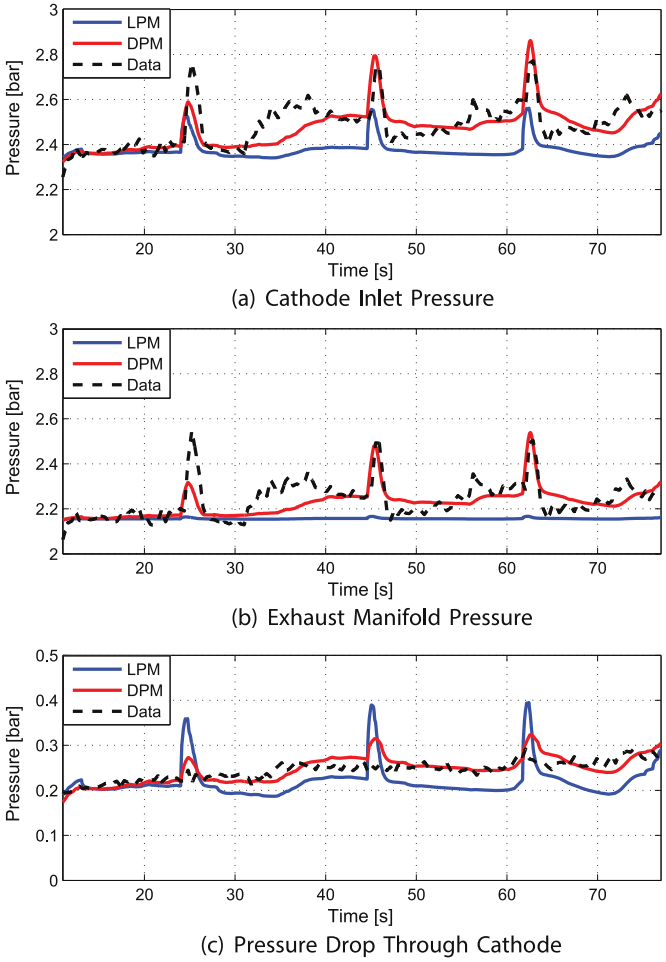

Fig. 17. Comparison of LPM and DPM predictions: validation results. (a) Cathode inlet pressure, (b) exhaust manifold pressure, (c) pressure drop through cathode.

Fig. 15 summarizes the results for the two models. The simplified cathode model based on [38] generally captures the magnitude of the pressure drop during sustained operations, especially during the initial part of the test. However, it fails to characterize the pressure drop growth caused by the accumulation of liquid water in the channels, which progressively obstructs the gas flow.

This is confirmed by comparing the predicted exhaust manifold pressure of the two models, as shown in Fig. 15(b). Since the flow of Heliox to the stack is constant during the test, the pressure predicted by the simplified model is nearly unchanged, since the flow rate through the restrictions is not affected by the presence of liquid water, but only by the composition of the exhaust gases.

The limitations of the simplified model are evident in this example. The assumption of ignoring liquid water may be reasonable for lower power fuel cell systems, or systems operating at lower current density. However, a prediction of the liquid water transport and its influence on the cathode pressure becomes critical for the high power system of the BB2, where a large amount of current is being generated. This is exemplified in Fig. 16, where the mass of water produced during the test is compared to the prediction of the DPM. During the test, nearly 4 kg of water are generated by the two fuel cell modules and expelled at the exhaust.

Table 4 summarizes the mean error, calculated by Equation (22), for the two models and the number of state variables in each model. In addition, an evaluation of the computation time was provided by running the two models at a fixed time step of 10 ms on a single-core Intel i5 processor with 4 GB RAM.

As expected, the DPM achieves better accuracy in predicting the slow increment of the cathode back pressure caused by the water transport dynamics. On the other hand, the computation time is also increased (while still being faster than real time), due to the increased number of states introduced by the cathode water transport model and the nonlinear inlet and outlet manifold resistance equations.

5.2. Validation results

A validation of the two models was conducted by imposing the current profile shown in Fig. 14(b), hence introducing the rapid transients corresponding to the gear shifts. As mentioned for the calibration test, only the central portion of the test data is considered for the validation of the two models, neglecting the startup and shut down transients.

As shown in Fig. 17, the presence of the gear shifts leads to three distinct spikes in the cathode pressure profile, caused by a temporary drop of the oxygen consumption inside the channels that forces higher gas flow rate through the exhaust.

In Fig. 17(a), the LPM is able to capture pressure spikes at each shift, however without a match on their magnitude. Similar to the calibration test, the error in predicting the slow increase in the

Table 5
Comparison of LPM and DPM performance for validation set (Fig. 14(b); test duration: 80 s).

	Error on inlet pressure (bar)	Error on exhaust pressure (bar)	Error on pressure drop (bar)	Comp. time (s)
LPM	0.112 (4.5%)	0.087 (3.8%)	0.038 (12.6%)	2.4
DPM	0.049 (2.0%)	0.045 (1.9%)	0.014 (4.6%)	14.4

cathode pressures caused by the liquid water buildup is also observed.

On the other hand, the DPM captures the magnitude of the pressure spikes, as well as the growth of the cathode inlet pressure. On the other hand, modeling error is evident immediately after the first gear shift, where the experimental data show a sudden increase in the cathode inlet and exhaust manifold pressures that may be caused by an adjustment in the BPV position that is not captured in the two models (the dynamics of the spring-diaphragm actuator was neglected).

Fig. 17(c) compares the cathode pressure drop traces predicted by the two models with the experimental data. The LPM, due to the inability to predict the effects of the liquid water on the exhaust manifold pressure, tends to systematically overestimate the magnitude of the peak pressures. Conversely, the DPM shows a consistent match of the experimental data, capturing well both the slow rate of pressure increase and the rapid spikes during the gear shift transients.

As a confirmation of the improved accuracy of the DPM, the mass of water produced during the test was measured and compared to the model prediction. The results, shown in Fig. 18, prove that the quantity of water generated is tracked well by the model.

Finally, Table 5 summarizes the mean absolute error for the two models and compares the computation time.

The validation results confirm the ability of the DPM to accurately track the water transport in the cathode channels and its effects on the cathode pressure dynamics, representing a significant advantage over the simplified control-oriented models, such the LPM.

In light of control applications, both the simplified LPM and the more accurate DPM could be directly implemented into an open-loop control strategy to provide an anticipatory control action at each gear shift, compensating the pressure spikes by opening the pressure relief valves. However, the systematic underestimation of the cathode pressure spikes caused by the LPM may result in the failure of a seal, with major consequences on the performance and safety of the fuel cell system. Conversely, an overestimation of the pressure drop may result in an excessive opening of the PRVs, with a consequent venting of gases and loss of power. For the above reasons, the DPM appears as a better candidate for the development of control strategies to manage the cathode pressure.

6. Conclusions

This paper presents a novel control-oriented model of the cathode pressure dynamics in a high performance PEM fuel cell. The case study considered is the Buckeye Bullet 2, the world's fastest hydrogen fuel cell vehicle. In order to generate the 540 kW power necessary for a 90 s speed run, a unique gas supply system was designed to feed high-pressure Heliox with 40% oxygen content to the cathode. Due to the high current density, considerable amount of water is generated in the cathode channels, with critical effects on the stack pressure and pressure drop.

Initially, a well-established lumped-parameter model was applied to predict the cathode pressure dynamics of the BB2 fuel cell system. However, the intrinsic limitations of this approach (particularly, the independence of the cathode pressure drop from the liquid water formed in the GDL), led to the design of a novel distributed-parameter model, which predicts the water formation and transport in the cathode channels based on the conservation laws for viscous fluid flows.

The resulting model was calibrated and validated on experimental data, collected on a laboratory setup designed to simulate the typical usage conditions that the Buckeye Bullet 2 fuel cell system would experience during a race. The cathode pressure model was benchmarked against the experimental data and compared to the prediction of the simplified lumped-parameter model.

The results presented show that the distributed-parameter model offers a significant improvement over the lumped-parameter model in the ability to predict the pressure dynamics at high current density conditions, due to the physics-based characterization of the liquid and gas flow in the cathode channel, and the inclusion of pressure drop models that account for the two-phase nature of the flow. While small modeling errors have been observed, they could be easily addressed by improving the model of the BPV actuator. Similarly, the structure of the model could be improved by including a more rigorous description of the water evaporation and condensation dynamics within the cathode. the validity of the model is limited to a case with near-constant stack current, the results shown can easily be extended to include different operating conditions. Nevertheless, the model presents a trade-off between accuracy and computational complexity that makes it favorable for the design of control algorithms to monitor the stack pressure. In this sense, the system-level model developed can be a powerful tool to facilitate the transfer of information between the stack manufacturers and the system integrators, and assist in system design, optimization and control design for the complete system.

Acknowledgment

The availability of this unique data set and system was made possible by the hard work of many members of the BB2 team who volunteered while being full time students. The authors are grateful to the many sponsors of the program, and particularly to Ballard Power Systems, Ford Motor Company and Venturi Automobiles for their support.

References

[1] J. Amphlett, R. Baumert, R. Mann, B. Peppley, P. Roberge, Journal of the Electrochemical Society 142 (1) (1995) 9–15.
[2] R. Mann, J. Amphlett, M. Hooper, H. Jensen, B. Peppley, P. Roberge, Journal of Power Sources 86 (2000) 173–180.
[3] J. Amphlett, R. Baumert, R.F. Mann, B. Peppley, Journal of the Electrochemical Society 142 (1) (1995) 1–8.
[4] J. Amphlett, R. Mann, B. Peppley, P. Roberge, A. Rodriques, A practical PEM fuel cell model for simulating vehicle power sources, in: Proceedings of Battery Conference on Applications and Advances, 1995.
[5] J. Amphlett, R. Mann, B. Peppley, P. Roberge, A. Rodriques, Journal of Power Sources 61 (1996) 183–188.
[6] M. Fowler, R. Mann, J. Amphlett, B. Peppley, P. Roberge, Journal of Power Sources 106 (2002) 274–283.
[7] R. Mann, J. Amphlett, B. Peppley, C. Thurgood, Journal of Power Sources 161 (2006) 775–781.
[8] A. Rowe, X. Li, Journal of Power Sources 102 (2001) 82–96.
[9] M. Verbrugge, R. Hill, Journal of the Electrochemical Society 137 (12) (1990) 3770–3771.
[10] D. Bernardi, M. Verbrugge, Journal of the Electrochemical Society 139 (9) (1992) 2477–2491.
[11] T. Nguyen, R. White, Journal of the Electrochemical Society 140 (8) (1993) 2178–2186.
[12] M. Perry, J. Newman, E. Cairns, Journal of the Electrochemical Society 145 (1) (1998) 5–15.
[13] A. Weber, R. Darling, J. Newman, Journal of the Electrochemical Society 151 (10) (2004) A1714–A1727.

[14] A. Weber, J. Newman, Chemical Reviews 104 (2004) 4679–4726.
[15] A. Biyikoglu, International Journal of Hydrogen Energy 30 (2005) 1181–1212.
[16] D. Cheddie, N. Munroe, Journal of Power Sources 147 (2005) 72–84.
[17] C.-Y. Wang, Chemical Reviews 104 (10) (2004) 4727–4766.
[18] H. Voss, D. Wilkinson, P. Pickup, M. Johnson, V. Basura, Electrochimica Acta 40 (3) (1995) 321–328.
[19] P. Sauriol, G. Kim, H. Bi, J. Stumper, J. St-Pierre, Comparison Between PEMFC Water Management Model and In-situ Water Transfer Measurements, AICHE, 2005. (Annual Meeting).
[20] T.R. Ralph, G.A. Hards, J.E. Keating, S.A. Campbell, D.P. Wilkinson, M. Davis, J. St-Pierre, M.C. Johnson, Journal of the Electrochemical Society 144 (11) (1997) 3845–3857.
[21] K. Promislow, B. Wetton, IAM Journal of Applied Mathematics 70 (2) (2009) 369–409.
[22] J. Stumper, H. Haas, A. Granados, Journal of the Electrochemical Society 152 (4) (2005) A837–A844.
[23] P. Berg, K. Promislow, J. St-Pierre, J. Stumper, B. Wetton, Journal of the Electrochemical Society 151 (3) (2004) A341–A353.
[24] J. Stumper, M. Lohr, S. Hamada, Journal of Power Sources 143 (2005) 150–157.
[25] P. Berg, A. Caglar, K. Promislow, J. St-Pierre, B. Wetton, IMA Journal of Applied Mathematics 71 (2006) 241–261.
[26] P. Chang, J. St-Pierre, J. Stumper, B. Wetton, Journal of Power Sources 162 (2006) 340–355.
[27] Jürgen Stumper, Charles Stone, Journal of Power Sources 176 (2) (2008) 468–476.
[28] P. Chang, G. Kim, K. Promislow, B. Wetton, Journal of Computational Physics 223 (2007) 797–821.
[29] B. Wetton, K. Promislow, A. Caglar, A simple thermal model of PEM fuel cell stacks, in: Second International Conference on Fuel Cell Science Engineering and Technology. Keith Promislow, Brian Wetton, Journal of Power Sources 150 (2005) 129–135.
[30] Y. Wang, S. Basu, C. Wang, Journal of Power Sources 179 (2008) 603–617.
[31] U. Pasaogullari, W. Chao-Yan, Journal of the Electrochemical Society 152 (2) (2005) A380–A390.
[32] G. Lin, W. He, T. Van Nguyen, Journal of the Electrochemical Society 151 (12) (2004) A1999–A2006.
[33] L. Zheng, A. Srouji, A. Turhan, M. Mench, Journal of the Electrochemical Society 159 (7) (2012) F267–F277.
[34] T. Springer, T. Zawodzinski, S. Gottesfeld, Journal of the Electrochemical Society 138 (8) (1991) 2334–2342.
[35] Thomas F. Fuller, John Newman, Journal of the Electrochemical Society 140 (5) (1993) 1218–1225.
[36] S. Mazumder, Journal of the Electrochemical Society 152 (2005) A1633–A1644.
[37] D. Ambühl, N. Anguiano, M. Sorrentino, Y. Guezennec, S. Mazumder, G. Rizzoni, A reduced 1 & 1D model for optimization analysis of a PEM fuel cell, in: Proceedings of ASME International Mechanical Engineering Congress and Exposition (IMECE2005-80121), 2005.
[38] J. Pukrushpan, A. Stefanopoulou, H. Peng, Control of Fuel Cell Power Systems, Springer, 2005.
[39] J. Pukrushpan, H. Peng, A. Stefanopoulou, Transactions of the ASME 126 (2004) 14–25.
[40] J. Pukrushpan, A. Stefanopoulou, H. Peng, Control of fuel cell breathing, IEEE CSM, April 2004, pp. 30–46.
[41] S. Gelfi, A. Stefanopoulou, J. Pukrushpan, H. Peng, Dynamics of low-pressure and high-pressure fuel cell air supply systems, in: Proceedings of the American Control Conference.
[42] X. Xue, J. Tang, A. Smirnova, R. England, N. Sammes, Journal of Power Sources 133 (2004) 188–204.
[43] J. Larminie, A. Dicks, Fuel Cell Systems Explained, John Wiley & Sons, 2005.
[44] R. Sonntag, C. Borgnakke, G. Van Wylen, Fundamentals of Thermodynamics, Wiley, 1998.
[45] R. Fox, A. McDonald, Introduction to Fluid Mechanics, fifth ed., Wiley, 1998.
[46] L. Tong, Y. Tang, Boiling Heat Transfer and Two-Phase Flow, Taylor & Francis, 1997.

Nomenclature

F: Faraday constant
h,H: height
I: current
K: pressure drop coefficient
m: mass
M: molecular weight
n: moles of electrons produced per mole of hydrogen reacted
P: pressure
Q: volumetric flow rate
R: specific gas constant
t: time
T: temperature
u,U: flow velocity
V: volume
w: width
W: mass flow rate
X: mass fraction
α: slip factor
ϕ: relative humidity
μ: dynamic viscosity
ρ: density
Ω: resistance

Subscripts
g: gas
h: Heliox
L: water–liquid phase
o: oxygen
v: water–vapor phase